New Journal of Physics
The open-access journal for physics

Detection of charge motion in a non-metallic silicon isolated double quantum dot

T Ferrus[1], A Rossi, M Tanner, G Podd, P Chapman and D A Williams

Hitachi Cambridge Laboratory, J J Thomson Avenue, Cambridge CB3 0HE, UK
E-mail: taf25@cam.ac.uk

New Journal of Physics **13** (2011) 103012 (21pp)
Received 23 June 2011
Published 11 October 2011
Online at http://www.njp.org/
doi:10.1088/1367-2630/13/10/103012

Abstract. As semiconductor device dimensions are reduced to the nanometer scale, the effects of high-defect-density surfaces on the transport properties become important to such an extent that the metallic character that prevails in large and highly doped structures is lost and the use of quantum dots for charge sensing becomes complex. Here, we have investigated the mechanism of the detection of electron motion inside an electrically isolated double quantum dot that is capacitively coupled to a single-electron transistor (SET), both fabricated from highly phosphorus-doped silicon wafers. Despite the absence of direct charge transfer between the detector and the double dot structure, efficient detection is obtained. In particular, unusually large Coulomb peak shifts in gate voltage are observed. The results are explained in terms of charge rearrangement and the presence of inelastic cotunneling via states at the periphery of the SET dot.

[1] Author to whom any correspondence should be addressed.

Contents

1. Introduction

Early experiments on charge quantization in tunnel junctions [1] initiated the development of single-electron tunneling devices. However, not until the theoretical work of Averin on Coulomb oscillations (COs) [2] and the improvement of electron beam lithography were single-electron transistors (SETs) fabricated [3]. The ability of SETs to detect the transfer of a single electron via Coulomb blockade (CB) with a high efficiency made them usable in many architectures as charge pumps [4], single-electron memories [5], quantum cellular automata [6] or in quantum computation [7] as charge detectors. For ease of operation, as well as for reliability, these nanometer-scale transistors are designed to have a metallic character. In particular, irregularities in the confining potential are screened so that the internal electronic structure is well represented by energy levels whose separation is defined by the dot diameter. In such *metallic* dots, localized states play a negligible role in the transport, and sequential tunneling events are well predicted by the orthodox theory of CB [8], which relates the electron dynamics to bi-dimensional electron gas systems.

The *metallic* property of the SET could be controlled by various methods, among which the most commonly implemented ones are the use of a central metal island and metal oxide tunnel barriers, as in $Al/Al_2O_3/Al$ SETs [9], the patterning of depletion gates in GaAs-based detectors [10] or the realization of a metal oxide–semiconductor (MOS) structure, as in fin field effect transistor devices (FinFET) [11] or in nanowire-based SETs [12]. Nevertheless, the sensitivity of *metallic* SETs is limited by the $1/f$ noise due to charge fluctuations at the dielectric–metal interfaces (Al/Al_2O_3) or trap charges (Pb1 centers) at the $Si/SiO_2(100)$ interface in MOS structures. This explains why high-frequency measurement or synchronous detection by two independent SETs may need to be performed to reduce the noise level [13].

If a MOS structure is not used, silicon has to be doped to a high level and constrictions have to be patterned to help in controlling the location of formation of tunnel barriers [14]. In such a small system, randomness in dopant distribution and surface roughness could be responsible for device instabilities at low temperatures. Indeed, localized states that may be present, especially at the edge of the device, are sensitive to variation in the electrostatic potential. The problem of knowing the specific local potential within a non-bulk semiconductor nanostructure remains a challenge for many types of device, so the recognition of process-dependent characteristics is useful in obtaining indirect information about that potential.

When used as detectors, SETs are generally electrically coupled to a device made of a single or a double dot that is directly or indirectly connected to source and drain contacts [15]. All these architectures are generally thought to be efficient in terms of charge detection owing to the strong coupling between the tunneling electron and the detector. Nonetheless, the back-action from the detector to the device is substantial and electrical connections to the device and/or between the SET and the device are a non-negligible source of noise. In contrast, the use of a geometrically isolated structure but capacitively coupled to the detector improves the electrical isolation but makes the detection more difficult. However, if these localized states at the detector edge could be controlled by geometric or electrostatic means, then they may be used to enhance the detection or to detect weaker effects.

In this paper, we investigate a structure made of highly phosphorus-doped silicon and comprising an isolated double quantum dot (IDQD) with a capacitively coupled SET. In such a device, the edge states occupancy could be modified by geometrical or electrostatic means, so that the coupling strength between the detector and the double dot structure could be engineered, leading to efficient detection of electron motion in the IDQD. Observation of Coulomb peak shifts in gate voltage as well as cotunneling gives insight into the complex electron dynamics in this system and the important role played by edge-localized states.

We first briefly introduce the device structure and the measurement setup. In section 3, we describe the observation of IDQD lines in a gate stability diagram and present a first attempt at simulating the experimental data and at describing the charge state dependence on gate voltages in the IDQD–SET system. In section 4, we discuss the detection mechanism in the SET by reviewing classical capacitance-based models and a trap-assisted tunneling model. This paper concludes with a summary in section 5.

2. Devices and measurement setup

The devices are fabricated from a silicon-on-insulator (SOI) wafer with a 45 nm thick silicon layer, doped with phosphor us at a density of $\sim 2.9 \times 10^{19}\,\mathrm{cm}^{-3}$. High-resolution electron beam lithography and reactive ion etching were used to pattern a single dot of diameter $\sim$75 nm with 30 nm wide tunnel barriers for the detector as well as an isolated double dot $\sim$75 nm in diameter. After oxidation the silicon dots were reduced to 60 nm in diameter with a lateral oxide thickness of 17 nm. The devices are controlled by three in-plane gates that are formed from the same SOI layer (figure 1), one controlling the SET and the other two controlling the double dot. The silicon substrate was connected to the ground. A custom low-temperature complementary metal oxide–semiconductor circuit (LTCMOS) is used to provide the various voltages to the device and to measure the SET current through a charge integrator. This arrangement enabled an efficient noise gain suppression by using shorter cabling between the measurement circuit and the device, as well as sensitive and fast current detection, compared to

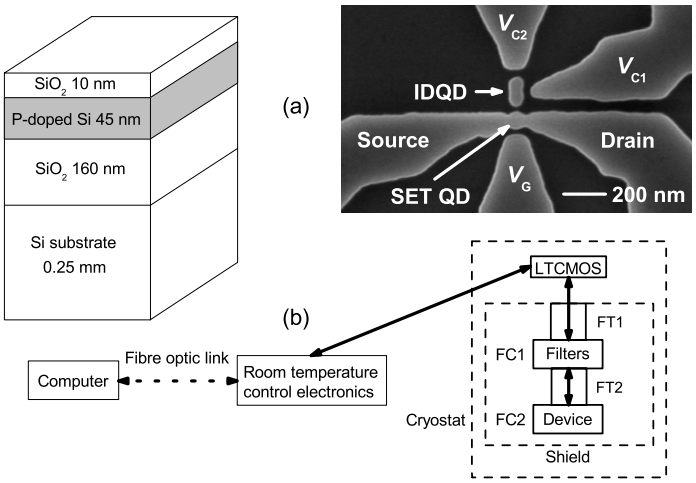

Figure 1. (a) Device structure and scanning electron microscope (SEM) image of the double dot with the nearby SET after oxidation. The upper IDQD gate was not fully functional and was grounded. (b) Schematic representation of the measurement setup using the LTCMOS, Faraday cages (FC1 and FC2) and feedthrough ferrite beads (FT1 and FT2).

conventional measurements using room-temperature source-measure units [16]. All lines were filtered by single-stage low-pass resistance–inductance–capacitor filters with a cut-off of about 80 kHz to suppress electrical noise and minimize the electron heating. The device and the filters are protected from radiated electrical noise by Faraday cages. Both the device and the LTCMOS were kept at 4.2 K by immersing the probe into liquid helium. Several devices were processed identically with similar dimensions, some from different wafers. All showed similar characteristics and behavior at low temperature or during thermal cycling.

3. Isolated double quantum dot (IDQD) charge state detection

In order to gain insight into the mechanism of charge motion detection in the IDQD, we have measured the dependence of the SET source–drain current I_{SD} on the SET gate (V_G) and IDQD gate voltages (V_{C1} and V_{C2}) (figure 2). In the interest of simplifying the data analysis, V_{C2} (figure 1(a)) was grounded in most experiments. If not, its voltage was kept within the range $-0.9\,\text{V} < V_{C2} < 0.5\,\text{V}$ to avoid gate leakage. The obtained gate stability diagram I_{SD} (V_G, V_{C1}) clearly shows the existence of regions of gate voltages with anomalously low or high current, which are associated with the presence of localized states in the device, as well as the usual COs (SET lines). Both features are detailed in appendices A and B, respectively. Additional features associated with the presence of the IDQD are also observed and discussed in the following sections.

3.1. IDQD lines

A common observation in these devices is the presence of additional lines in the gate stability diagram with a slope steeper than those associated with the SET (figure 2(a)). When intersecting the COs, these lines either enhance the Coulomb peak conductivity at specific gate voltages

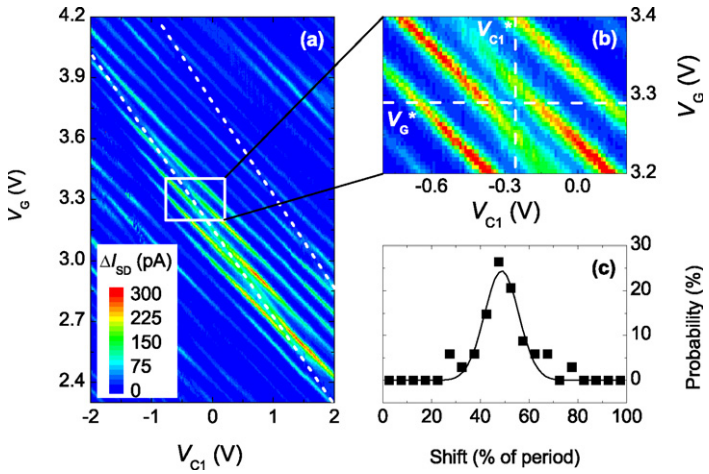

Figure 2. (a) Gate stability diagram with CO and IDQD lines (dotted lines). (b) Shift as seen at the intersection between SET and IDQD lines. (c) Distribution of the value of shift as a percentage of the CO period taken from different devices, cooldown and gate voltages. The most probable value is 49%.

($V_G^\star$ and $V_{C1}^\star$) or locally split them into two branches ($V_{C1} < V_{C1}^\star$ and $V_{C1} > V_{C1}^\star$) separated by a region of low but finite conductivity. On each branch, the Coulomb peak is shifted from its normal position by about $25 \pm 7\%$ of the CO period (figure 2(c)).

Unlike COs, the additional lines are not periodic. Their position and visibility are both strongly affected by thermal cycles, but their slope is almost constant ($dV_G/dV_{C1} \sim 0.43 \pm 0.05$). They are always present in devices containing an IDQD but are never observed otherwise. Still, associating these lines with the IDQD requires a deeper analysis because of the absence of a direct electron transfer from the IDQD to the detector, and so, of the impossibility of observing hexagonal shapes in the gate stability diagram, as usually obtained in connected double quantum dots.

The presence of additional conductivity lines in stability diagrams has been referenced by a few authors. In GaAs/GaAlAs quantum dots [17] they have been related to bound electrons at the periphery of the quantum dot when the device is tuned to be close to the delocalization–localization transition, e.g. a situation where both localized electrons at the dot boundary and delocalized electrons at the center of the island coexist. Further observations have been made by Gunther *et al* [18], this time in a silicon metal oxide–semiconductor field effect transistor (MOSFET)-like structure. In that paper, an alternative explanation is given and additional lines are expected to result from a modification of the quantum dot confinement that lifts the degeneracy of the quantized energy levels.

In both cases, these features originate from the specific internal electronic structure of the quantum dot. Although regions of different localization strengths do exist in our devices, there are a number of differences. Firstly, in Zhitenev's device, anticrossings are visible at the intersection between additional and SET lines. This means that there is no discontinuity in the Coulomb peak positions in gate voltage, and so no noticeable variation of the peak capacitance over the transition region. The peak position is not altered or is only changed by a few per cent at either side of the crossing point. In contrast, we do observe a clear discontinuity (or shift) in the Coulomb peak position in gate voltage, as well as a strong variation in the conductivity at

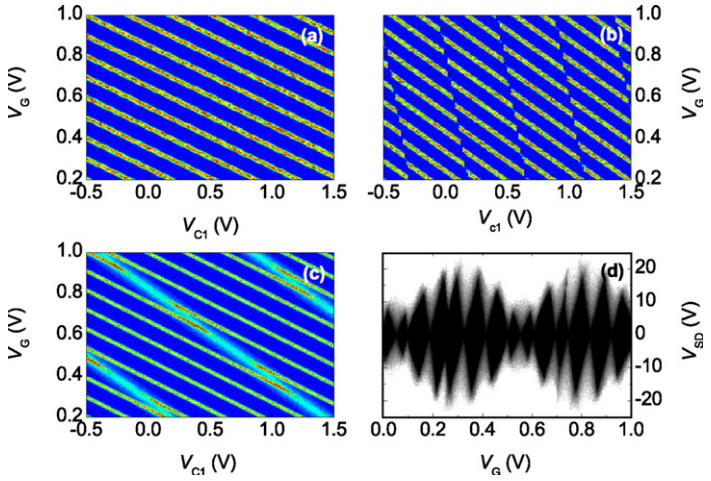

Figure 3. Gate stability diagrams in the case of a SET alone (a), a SET connected to a single dot via a tunnel barrier (b) and a SET with a capacitively coupled IDQD (c). (d) Coulomb diamonds obtained adding a parallel conduction mechanism in the case of a SET–IDQD structure.

the crossing point. Secondly, the slope of the additional lines is, in our case, almost constant over a wide range of gate voltages, unlike Zhitenev or Gunther's observations.

Sharp and clear shifts have been observed in a doubly gated planar silicon MOS structure in the accumulation mode by Morello *et al* [19]. In their experiments, the line slope $\mathrm{d}V_\mathrm{G}/\mathrm{d}V_\mathrm{C1}$ is very large, a distinctive feature of random telegraph signal or electron tunneling from an impurity outside, but close to, the detector edge into the detector itself. However, the edge of our SET has been electrically isolated by etching the surrounding silicon, so such a tunneling is unlikely.

3.2. IDQD coupling and trap-assisted tunneling: simulations

In order to establish the origin of the observed additional lines, we performed first-principle calculations and simulations using SIMON 2.0, a single-electron circuit simulator based on Monte Carlo simulation [20]. Although neglecting the shape of the dots, the dopant distribution and many-body interaction, these simulations give substantial indications of the structure responsible for the additional lines.

Simulations that include an SET without an IDQD reproduce the characteristic slope of the SET lines in the gate stability diagram well (figure 3(a)). In simulations where an SET is connected via a tunnel barrier to a nearby trap charge, additional lines are obtained but with a slope $\mathrm{d}V_\mathrm{G}/\mathrm{d}V_\mathrm{C1} \gg 1$, similarly to the work of Morello *et al* (figure 3(b)) but unlike our experimental results.

However, the values for the SET and additional line slopes as well as for the shift were reproduced well when considering a SET that is capacitively coupled to a double dot system. Simulations also reveal that the IDQD is modeled better by a single but large dot where electrons are allowed to move between the lower and the upper IDQD dots via a tunnel barrier. This behavior is expected from the width of the tunnel barriers, the orientation of the IDQD with respect to the SET and gates, as well as from the size of the dots measured by SEM. The

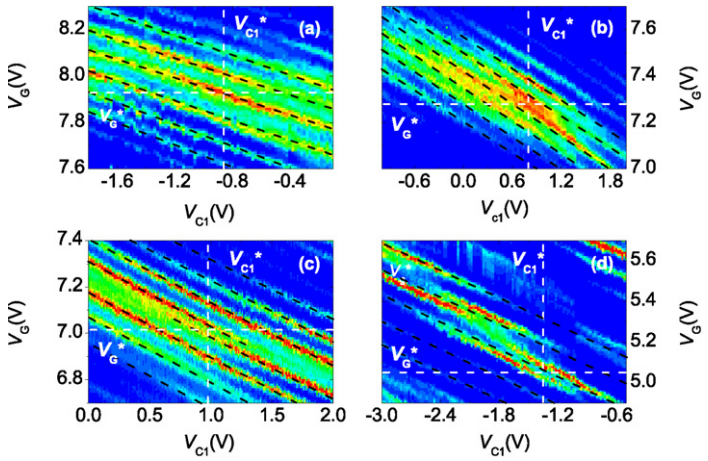

Figure 4. Effects of the coupling strength between the IDQD and the SET on the SET current, from weak coupling (a) to strong coupling (d).

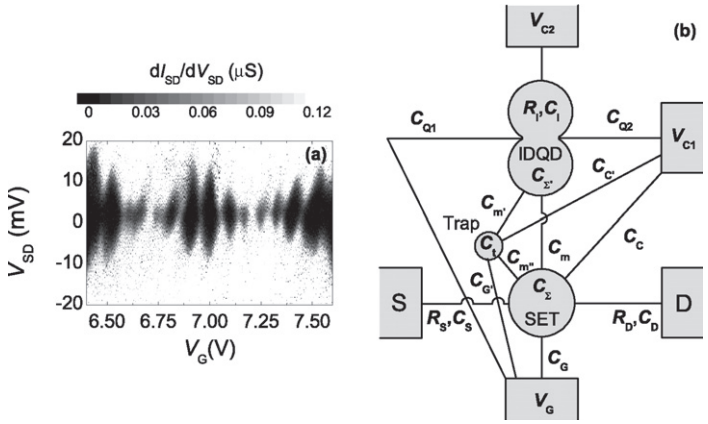

Figure 5. (a) Coulomb diamonds showing parallel dot-like behavior. (b) Schematic diagram for the capacitance and resistance circuit used for the simulations with a SET, an IDQD and a trap charge as well as the different gates and the source (S) and drain (D) contacts. For clarity not all capacitances are shown.

tunneling resistance between the two IDQD dots governs the visibility of the region around the shift, whereas the intra-IDQD and SET–IDQD capacitance influence the value of the shift itself.

Indeed, in such a structure, the electrostatic environment is modified by the different voltages applied to it with a strong interplay of impurities and charge reorganization (appendix A). As a result, we expect capacitances to be gate voltage dependent. Such a variation in the inter-dot coupling strength is clearly revealed in figure 4.

However, simulations failed to reproduce correctly a number of features in the current–voltage dependences. The most striking is the shape of Coulomb diamonds. Experimentally charging energies vary strongly with gate voltages and the extent of the Coulomb diamond along V_{SD} may be noticeably reduced in some regions (figure 5(a)). This effect can qualitatively be taken into account by adding a parallel tunneling process via a trap

Table 1. Values for capacitances (aF) and resistances (kΩ) as defined in figure B.2(d).

C_G	C_C	C_{Q1}	C_{Q2}
1.61	0.471	0.77	0.34
$R_{S(D)}$	$C_{S(D)}$	R_i	C_i
133	8	200	0.4
C_m	$C_{m'}$	$C_{m''}$	
0.8	0.2	0.2	

charge in the SET. The trap is simulated as a quantum dot connected to the SET and contacts via a tunnel barrier and capacitively coupled to the IDQD (figures 3(c) and (d)). Such a trapping mechanism also explains the local increase in conductivity well, controlled by the tunneling resistance between the contacts and the trap, and the broadening of the Coulomb peak at the shift position, controlled by the coupling capacitance between the trap and the IDQD (figure 3(c)).

Figures 2(a) and 5(a) (appendix B) were used for simulations, and the gate dependences of the current were fitted well using the capacitance values listed in table 1.

The capacitance values agree well with those obtained from FastCap 2.0 software [21], which is used to compute the self- and mutual capacitances of a conductive tri-dimensional structure, whose dimensions were extracted from SEM imaging.

3.3. Charge states in the IDQD–single-electron transistor (SET)-trap structure

Although simulations satisfactorily explain experimental data and link the observation of additional lines to the presence of the IDQD, a few inconsistencies suggest that a more sophisticated model may be needed. For example, in figure 4(d) the SET lines have their conductivity strongly suppressed away from the shift position. Also, these lines do not deviate from their original position except at the intersection with the IDQD lines (local shift), in contrast to the simulations, where all SET lines are shifted together after the crossing (global shift). This might suggest a stronger influence of traps on the SET dynamics and the possibility of electron correlation.

Indeed, SIMON 2.0 allows electron transfer to the trap and the SET at the same time without taking into account that a filled trap at the edge of the SET or close to the barrier may block further tunneling into the SET island due to Coulomb repulsion. This is because both the SET and the trap are considered as two separate structures. It is possible to improve the modeling by considering that the trap charges are located within the SET, so that the total charge of the SET and the trap has to be maintained constant in a blockade region.

In a system made of a SET with a capacitively coupled IDQD, the dependence of the Coulomb peak position on gate voltage can be determined approximately without involving lengthy capacitance matrix calculations by noting that a change in the bias condition $\mathrm{d}V$ is equivalent to a charge addition $\mathrm{d}Q = C\mathrm{d}V$ in the structure and that a variation of charge $\mathrm{d}Q'$ in the IDQD modifies the potential in the SET, leading to an effective charge addition in the detector of $\mathrm{d}Q'' = C_m/C_{\Sigma'}\mathrm{d}Q'$, where C_m is the capacitance between the SET and the IDQD and $C_{\Sigma'}$ the total capacitance of the IDQD. Similarly to the SET lines, IDQD lines correspond to a tunneling of an electron between the two IDQD dots through the tunnel barrier separating them.

By neglecting back-actions between the SET and IDQD and following the previous comments on charge tunneling, the SET lines are given by

$$V_G \approx -\frac{C_C}{C_G} V_{C1} + \frac{e}{C_G} N_S + \frac{eC_m}{C_{\Sigma'} C_G} N_i \tag{1}$$

and the IDQD lines by

$$V_G \approx -\frac{C_{Q2}}{C_{Q1}} V_{C1} + \frac{e}{C_{Q1}} N_i + \frac{eC_m}{C_\Sigma C_{Q1}} N_S, \tag{2}$$

where e is the elementary charge and N_S and N_i are the total numbers of electrons in the SET and IDQD, respectively. Other notations are defined in figure 5(b).

The first terms in equations (1) and (2) give the corresponding slopes in the gate stability diagram, whereas the second terms give the period on the V_G axis and the third terms the shift in gate voltage relatively to the *ideal* position (without the capacitively coupled structure).

Because of the absence of electrical connections between the IDQD and the source or drain leads, $C_\Sigma \gg C_{\Sigma'}$, so that experimentally the IDQD lines are not significantly shifted when intersecting the SET lines. Unlike with SET lines, we did not observe any periodicity in the IDQD lines experimentally. This may indicate that more complex mechanisms involving traps at the SET periphery and Coulomb interaction may be involved or, more directly, that capacitances, in particular C_m, may depend on gate voltages.

By taking into account a trap charge at the edge of the SET, the shift of the SET peak position (as a percentage of the CO period) is

$$\gamma = \Delta N_t \frac{C_{m''}}{C_t} + \Delta N_i \left(\frac{C_m}{C_{\Sigma'}} + \frac{C_{m'} C_{m''}}{C_{\Sigma'} C_t} \right), \tag{3}$$

where ΔN_t and ΔN_i are, respectively, the change in the number of electrons in the trap and in the IDQD.

Because the IDQD is electrically isolated from the rest of the device, its total charge, including localized and extended states, is conserved at all times. The SET conductivity can then be affected only if the coupling between the SET island and the IDQD quantum dots differs for the upper and lower dots, so that a charge displacement or a significant change in the electron distribution in the IDQD is seen, by the SET, as an effective charge offset ΔN_i in the IDQD structure. It should be noted that the perpendicular position of the IDQD relatively to the SET improves the difference in sensitivity of the two IDQD dots.

When following a Coulomb peak in the gate stability diagram but away from the crossing between the SET and IDQD lines, the charge is constant in the IDQD and there is a single tunnel event in the SET-trap system. Thus $\Delta N_i = 0$ and $\Delta N_t + \Delta N_S = 1$, with ΔN_S being the variation in electron number in the SET. In this case, either the electron tunnels to the SET island and $\gamma = 0$ (usual tunneling) or it tunnels to the trap and $\gamma = C_{m''}/C_t$ (trap-assisted tunneling). Because γ is independent of N_i, there is no global shift in the position of the SET line. However, at the shift position, $\Delta N_i = 1$, so that the SET lines are shifted by $\sim \pm C_m/2C_{\Sigma'}$ depending on the position of V_G and V_{C1} relatively to $V_G^\star$ and $V_{C1}^\star$. Finally, following the IDQD line ($\Delta N_i = 1$) but in the blockade region ($\Delta N_t + \Delta N_S = 0$), the increase of conductivity may result from cotunneling via the trap states (one electron tunneling to the trap and one electron leaving the SET island for charge conservation). In this case, cotunneling is expected to be inelastic due to the finite value of the trap binding energy. An estimated value for this energy is given in appendix C.

4. Detection mechanism

4.1. Classical models

Theoretical predictions that are based on purely static modeling, such as image charges, all predict a value for the shift close to 4 % of the CO period [22][2]. The model is based on the existence of interfaces and materials of different permittivities and neglects electron dynamics. It explains the experimentally measured value for the shift in the case of a mobile charge in nanocrystalline silicon quantum dots where detection is made by a multiple-gate SET [23], as well as in other *metallic*-like systems. This elementary model is also very suitable for capacitively coupled but weakly interacting systems [24] or for a similar system where the double quantum dot is parallel to the detector and connected to an electron reservoir [25].

This model is clearly unsuitable in our case for reasons discussed in the previous sections: in particular, the presence of a certain level of localization, the importance of tunneling via traps, as well as the isolated character of the IDQD. Indeed, if the IDQD was connected to a lead, then the effects of trapping and charge reorganization would have been significantly screened due to the continuous interaction between the electrons in the dots and those in the reservoir.

More sophisticated capacitance modeling, such as SIMON's, provided significant information on the dynamics of the system, but may not be entirely appropriate for a doped isolated structure. Indeed, traps are still simulated as *metallic* dots and electron interaction is neglected. This explains the inconsistency in the value of $C_{m''}$, which is expected to be large due to the strong coupling between trap and the SET island, although providing reasonable agreement with experimental data. Indeed, capacitance is irrelevant for such a localized state. Nevertheless, it is important to assess the extent of its validity. In such a model, quantum dot structures do not need to be explicitly electrically connected except when dealing with charge conservation. In particular, the voltage shifts between the SET lines can always be associated with a measure of the electrostatic coupling between the dots, including the case of an isolated structure such as the IDQD [26]. The equivalent coupling capacitance between the IDQD and SET is then given by

$$C_{m} = \gamma C_{\Sigma'}, \tag{4}$$

where γ is the Coulomb peak shift as a percentage of the CO period.

From section 3.3, we also have

$$\Delta = \frac{e}{C_{Q1}}, \tag{5}$$

$$S = -\frac{C_{Q2}}{C_{Q1}}, \tag{6}$$

where Δ is the separation between successive IDQD lines in gate voltage and S is their slope in the (V_g, V_c) gate dependence diagram.

[2] We consider an IDQD with permittivity ϵ_1, an SET dot with the same permittivity that is separated from it by a distance d and a medium of permittivity ϵ_2. A charge q located in the IDQD is then electrically equivalent to a charge $q' = (\epsilon_0/\epsilon_1)\,(\epsilon_2 - \epsilon_1)\,/\,(\epsilon_2 + \epsilon_1)$ in the SET, where ϵ_0 is the permittivity of vacuum. By taking $\epsilon_1 = 11.7$ and $\epsilon_2 = 1$, we obtain $q' \sim 0.07q$. Thus, a variation of the IDQD charge by q leads to a potential variation δV_G at the edge of the SET dot such as $\delta V_G = q'/(4\pi\epsilon_0 d) \sim 4.1$ mV or 4.3% of the CO period $\Delta V_G = 96$ mV.

From these relations, we obtain

$$C_{\mathrm{m}} = \frac{\gamma}{1-\gamma}\left[\frac{2e}{\Delta}(1-S)+C_{\mathrm{i}}\right], \tag{7}$$

γ and S being almost constant; the non-periodicity of the IDQD lines in gate voltage clearly shows that one has to consider the dependence of C_{m} on gate voltage.

By taking $\Delta = 0.207\,\mathrm{V}$ as the minimum observable value and $C_{\mathrm{i}} = 0.4\,\mathrm{aF}$, we obtain $C_{\mathrm{Q2}} \sim 0.33\,\mathrm{aF}$, $C_{\mathrm{Q1}} \sim 0.77\,\mathrm{aF}$, $C_{\Sigma'} \sim 2.34\,\mathrm{aF}$ and $C_{\mathrm{m}} \sim 0.84\,\mathrm{aF}$. However, for the maximum experimentally measured value, $\Delta = 0.453\,\mathrm{V}$, we have $C_{\mathrm{Q2}} \sim 0.15\,\mathrm{aF}$, $C_{\mathrm{Q1}} \sim 0.35$ aF, $C_{\Sigma'} \sim 1.91$ aF and $C_{\mathrm{m}} \sim 0.61$ aF. Good agreement is obtained between these experimental values and theoretical calculations when considering an effective relative permittivity of 2.1. This low value reflects that the SET and IDQD are surrounded by trenches filled, at low temperature, with liquid helium with permittivity close to 1. Although giving satisfactory results, this approach is an equivalent model for which the capacitance calculation is adjusted to an experimental observed value for the shift. Nevertheless, this model has the advantage of showing that the present experimental results cannot be understood without considering the dependence of the capacitance in gate voltage and possibly electron dynamics. This, in turn, confirms again the presence of a variable electrostatic environment, which is easily modeled by localized states at the edge of the SET, as previously discussed. It shall be noted that such a variable coupling is expected to strongly influence the SET gate capacitance C_{G} as well. In contrast, most of the variation in gate periodicity, with the exception of the Coulomb peak shift region, can be attributed to a variation in the value of the excited state energy so that C_{G} does not vary by more than 10% of its mean value. Indeed, the presence of a source and drain contact provides an equilibrium mechanism to the displacement of electrons inside the SET island, so that the variation in the electron distribution is compensated by electrons entering or leaving the SET island. This situation is very different in the double dot because of its insulation from the electrical environment, and such a compensation cannot take place. This coupling is generally weak, except when the electrostatic arrangement is favorable to a charge motion in the IDQD and its detection by the cotunneling effect in the SET island. This also suggests the possibility of charge rearrangement in both the IDQD and SET [27]. However, this model does not provide any information on the energies involved.

4.2. Charge ring model

Previous observations suggest that a significant proportion of traps and localized states are found at the periphery of the SET island (appendix A). Their distribution and the trap occupation number can eventually be controlled by fabricating a backgate and adjusting its voltage during the device cooldown. Such a method has already been applied successfully to MOS-based devices [28]. The presence of such a distribution of charge in a ring-like shape around a quantum dot was suggested by Zhitenev *et al* [17] and studied by Rudin *et al* [29] in floating gate transistors. Following the same method but adapting it to the present geometry, an electron getting trapped at the periphery of the SET island leads to a shift in gate voltage, from its normal position, given by

$$\delta V_{\mathrm{G}} = \frac{e}{\pi^2 \epsilon_0 \epsilon_r (r-R)} K\left[\frac{-4Rr}{(R-r)^2}\right], \tag{8}$$

where R is the SET radius including the silicon and oxide region, r is the distance from the center of the SET island to the edge of the SET gate, $\epsilon_r \sim 2.1$ is the effective permittivity of the trench and $K(x)$ is the complete elliptic integral of first kind.

Assuming that the trap is in the vicinity of the Si–SiO_2 interface, we take $R \sim 30$ nm and $r \sim 60$ nm (appendix B) and estimate that $\delta V_G \sim 25$ mV. This leads to a shift $2\delta V_G/\Delta V_G$ of about 51%, in excellent agreement with the experimental value. The large observed value is mostly due to the fact that the side gate and the SET island are electrically isolated by a trench. This may explain why such a large shift has never been observed in conventional gated devices where the permittivity is a factor of 10 higher.

Within this model, the energy necessary to trap one electron at the periphery is given by the mean single-particle level spacing Δ_1. This is confirmed by the presence of the central Coulomb diamond (I) in figure C.2(b) whose charging energy is about 1.8 meV and corresponds to the energy difference between the trapping of an extra electron and the removal of a trapped electron. It is interesting to note that when entering the dot the electron can tunnel into two possible states at E_C and $E_C + \Delta_1$. However, the $E_C + \Delta_1$ state has a stronger coupling to the edge states because the potential energy at the edge of the dot ($m^\star \omega_0^2 R^2/2$) corresponds to Δ_1, by definition. It is also the point where the kinetic energy is zero and so where the localized states are most likely to be. Such a coupling favors charge reorganization at a minimum cost within $e^2/(4\pi\epsilon r)\, e^{-\lambda r}$, where λ is the Thomas–Fermi screening length, when taking into account electron screening. Although the energy cost is higher via this process, the overall cost is lowered due to electron rearrangement so that the real cost in energy between the two processes, via normal tunneling and via cotunneling, is $\Delta E = \Delta_1 - e^2/(4\pi\epsilon r)\, e^{-\lambda r}$. The maximum value for r is the dot diameter corresponding to one electron being trapped at the source and one released at the drain so that $\Delta E = -0.2$ meV but values up to -2.3 meV could be obtained depending on the configuration.

4.3. Transport mechanism

It should be noted that the electron trapping mechanism at the periphery of the SET dot as described previously, as well as the value of the gate voltage shift given by equation (8), does not explicitly reference the presence of an IDQD, nor an electron displacement in the IDQD. However, in the absence of an isolated structure the effect is expected to be random, rare and generally hidden by direct electron tunneling, since it is a second-order tunneling process.

The presence of IDQD modifies the transport in different ways. When no electrons are transferred in the IDQD but the IDQD is polarized, the effective charge in the lower dot either suppresses the SET tunneling current by populating the SET periphery states, e.g reducing the effective dot size, or enhances the current in the blockade regime by displacing the electrons towards the inner region of the SET and minimizing scattering from localized electrons (appendix B.2). In addition, since the IDQD and SET are made from the same material with similar dimensions, the displacement of an electron in the IDQD induces both a charge reorganization in the IDQD and a modification of the electric field at the top of the lower IDQD dot. Due to capacitance coupling and under the appropriate gate voltages, the electrostatic potential is modified in the SET island with the strongest effect expected to happen at the periphery of the SET. This allows the trap occupation number to be modified at the edges

of the SET island at no energy cost, making cotunneling an efficient and dominant process (section 4.2).

Thus, the presence of a charge movement in an isolated structure provides a mechanism for the suppression of direct tunneling and the enhancement of trap-assisted cotunneling in the blockade regime, at specific and reproducible combinations of gate voltages, making the effect more visible and controlled. As a consequence, the direct observation of Coulomb peak shifts gives an indication of the effective polarization of the IDQD, $V_G^\star$ and $V_{C1}^\star$ indicating the gate positions of the IDQD state degeneracy.

5. Conclusions

We have shown that a highly phosphorus-doped silicon SET can efficiently detect charge movement in a nearby but electrically isolated double dot despite the absence of direct electron transfer between the two structures. The presence of localized states at the periphery of the SET dot and the ability of the system to proceed to charge rearrangement allow inelastic cotunneling to be an efficient conduction mechanism. In particular, the most noticeable effect is the presence of significant Coulomb peak shifts in gate voltage. In such devices, electron dynamics are complex. Nevertheless, the glass-like behavior of the systems allows charge reorganization to take place and detection to remain efficient. These results thus extend the possibility of realizing and detecting charge qubits in non-*metallic* devices.

Acknowledgments

This work was supported by Project for Developing Innovation Systems of the Ministry of Education, Culture, Sports, Science and Technology (MEXT) in Japan.

Appendix A. Impurities and localization

A.1. Conductivity background

The most noticeable feature in figure A.1 is the existence of a large conductivity background on top of which lie the usual COs. It is aperiodic and only reproducible within a single thermal cycle. This discards a purely electrostatic influence from the gate voltages or the creation of built-in potentials inside the structure. In contrast, this suggests the presence of charging effects and the probable influence of localized states. This effect was confirmed on all devices with or without the double dot structure.

The conductivity background is gate voltage-dependent, with regions where the SET current is anomalously suppressed and others where it is significantly enhanced. These features are found along lines with a slope $dV_G/dV_{C1} \sim 0.23 \pm 0.06$ in the gate stability diagram, a value close to the one observed for the COs. Therefore, it is likely that they originate from the main SET island.

Indeed, for a device containing traps, a thermal cycle allows electrons to be redistributed among localizing centers. So the electrostatic potential due to these charges is likely to be modified each time the device is thermally cycled (figure A.1(a) as compared with figure A.1(b)).

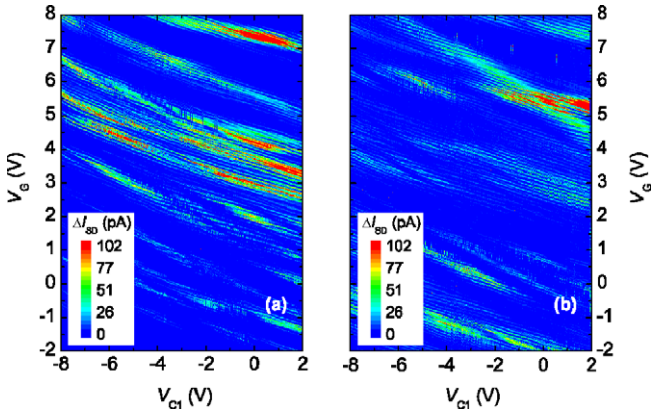

Figure A.1. Gate dependences following different cooldowns with a source–drain bias V_{SD}= 3 mV.

Because the IDQD is made of the same material than the SET, such a charge reorganization is also expected in the double dot structure. However, owing to its isolation from the rest of the device, it is difficult to probe separately the effect in the IDQD.

A.2. Localization

In doped semiconductors, the metallic phase is usually reached when the doping concentration exceeds the Mott critical limit n_C, i.e. when the impurity band merges into the conduction band. In the case of phosphorus-doped bulk silicon, $n_C \sim 10^{18}\,\mathrm{cm}^{-3}$ but, because of disorder, significant Lifshitz tails in the density of state remain up to about $4\times10^{19}\,\mathrm{cm}^{-3}$ as shown by Altermatt *et al* [30]. Therefore, localized states are still present above n_C but, because of their relative small number compared with extended states, they barely affect the conductivity that remains metallic. However, in reduced dimensions and, in particular, in quantum dots, the confinement increases electron–electron interaction and the presence of interfaces (especially non-(100) surfaces that are known to possess a high state density) play a significant role in the electron localization at the edge of the structure. In this case, Abrahams' scaling arguments and the concept of metal–insulator transition break down [31].

In our device, oxidation is used in order to reduce random telegraph signals and improve the noise performance. Nevertheless, this also redistributes phosphorus dopants towards the sidewalls of the structure, as demonstrated by the parabolic dopant profile obtained from secondary ion mass spectrometry (SIMS) experiments in similar devices [32]. The effective dopant concentration is then decreased at the center of the island. Segregation, a process highly dependent on oxidation conditions [33], may also happen and dielectric screening at the interface may contribute to the localization at the sidewalls, in a manner that is dependent on processing conditions.

The presence of impurity traps in a highly doped silicon device is thus not unusual. The existence of localized states was indeed demonstrated in microwave measurements and the temperature dependence of the conductivity [16]. Some weakly bound traps may be found inside the SET island. Still, most of the traps are expected to be found at the periphery of the SET island for the reasons given previously. It should be noted that localization effects barely affect the largest area of the device, including contact leads that keep their metallic behaviors.

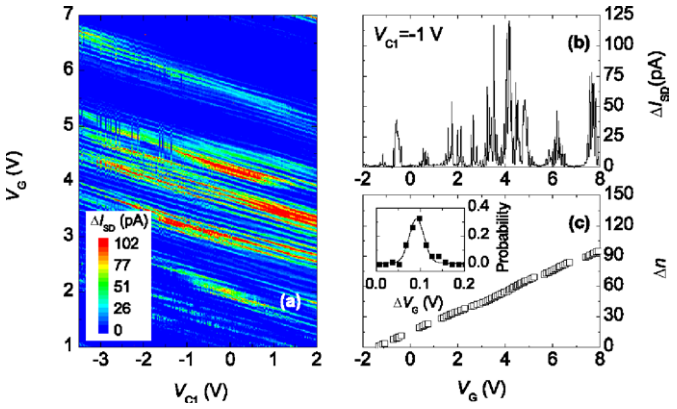

Figure B.1. (a) Variation of I_{SD} with V_G and V_{C1}. (b) SET gate oscillations for $V_{C1} = -1$ V. (c) Coulomb peak positions in gate voltage for $V_{C1} = 2$ V showing a clear periodicity with a relative small Gaussian dispersion (inset). Due to the increasing gate leakage current for $V_G < -2$ V, the SET could not be depleted and Δn represents the relative number of tunneling events in the SET island.

Appendix B. Detector properties

B.1. General characteristics

COs are clearly visible in the gate dependency diagram (figure B.1) as lines with a slope $dV_G/dV_{C1} \sim 0.25 \pm 0.01$. Deviations from the linear dependence are noticeable for the most negative IDQD gate values ($V_{C1} < -4$ V). In these regions, the leakage current is still relatively small as compared with I_{SD} but nonlinear effects in the structure may be induced at high voltages through a dependence of the capacitance values on gate voltages. The period of the oscillations ΔV_G remains close to 96 mV with no noticeable variation in gate voltage, and it is barely affected by thermal cycles. However, in all measured devices, the CO amplitude is strongly modulated by the conductivity background. The interplay between the COs and the conductivity background due to impurities is especially obvious when measuring the variation of the differential conductance with source–drain bias and observing the shape of the Coulomb diamonds (figure 5(a)). The latter are generally varying in dimensions and, in some cases, may appear as a convolution of diamonds of different sizes.

Still, such structures are not observed everywhere and, in regions of gate voltages that are weakly affected by impurities, diamonds have a more regular shape, similarly to what is expected for metallic devices (figure B.2). In such a region where the detector is behaving as a metallic-like island, capacitance approximation may be used and the information on the values of the capacitance between the different elements of the structure as well as an approximation to the dot dimension are possible.

The slope of the Coulomb peak position in the gate dependency diagram is then given by a capacitance ratio $\sim C_C/C_G$ where C_C is the IDQD side gate to SET island capacitance and C_G the SET gate to SET island capacitance (figure 5(b)).

For example, in the range $2.7\ V < V_G < 3.1\ V$ we obtain $C_G = 1.7 \pm 0.1$ aF and from the values of the level arms we find $C_D = 8.3 \pm 0.7$ aF and $C_\Sigma = 20.6 \pm 4.1$ aF, respectively, for the gate, drain and total SET dot capacitance. This gives a charging energy $E_C \sim 4.0 \pm 0.7$ meV

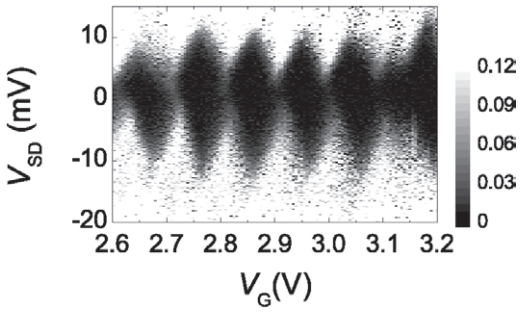

Figure B.2. Coulomb diamonds in undisturbed region for $V_{C1} = -3$ V.

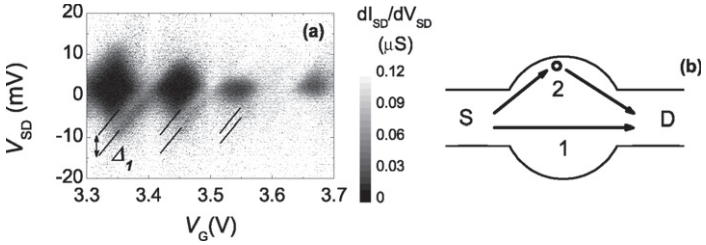

Figure B.3. (a) Excited states. Contrast had to be enhanced to obtain a measurable energy value for the smallest diamond). (b) Direct electron tunneling in the SET dot (1) between the source (S) and drain (D) contacts and possible parallel mechanism involving localized states at the dot periphery (2).

and a dot size of 32± 6 nm using the self-capacitance for a metallic sphere. The difference in diameter values between the one determined by SEM imaging (60 nm) and the one determined by electrical characterization may be caused by an enhancement of background charge-induced confinement [34].

B.2. Variable size quantum dot

As previously seen, the conductivity in the device is influenced by the presence of localized states, so that a correct determination of the dot diameter is, in general, difficult, in common with most semiconductor devices of this type. In some region of gate voltages, the appearance of convoluted diamonds suggest the existence of parallel conduction channels in some devices [35] (figure 5(a)). These parallel transport mechanisms may lead, in some cases, to the suppression of the SET current over a large range of gate voltage. It is strongly affected by thermal cycles, suggesting that conduction involves bound states in the SET island (figure B.3(b)) rather through a physically defined dot in the leads, barrier or inside the SET island. Following the discussion in appendix A, it seems reasonable to approximate the quantum dot as a metallic-like sphere surrounded by a region of stronger localization. Within this region, the electron redistribution may happen due to a change in temperature, such as during thermal cycling. At low temperatures, electron activation from traps is strongly reduced. However, the strength of both disorder and electron interaction may be sufficient to induce hopping between sites and to

allow a modification of the electrostatic environment following a change in the gate voltages. Indeed, the dimensionless parameter r_s[3] that characterizes the relative strength of the electron interaction is about 1 in our device. This indicates that both electron–electron interactions and disorder play an important role.

A parallel conduction mechanism or its suppression may be explained by a change in the trap occupancy inducing a modification of the confining potential. It will appear in regions where the donor binding energy allows hopping between localized sites to happen, so, most likely, at the periphery of the SET island. When all surrounding traps are occupied, the dot size is electrostatically reduced due to Coulomb repulsion and conduction via edge states is forbidden due to the absence of vacant sites. The Coulomb diamonds may then appear larger than expected. In contrast, if edge states are all empty then the effective dot size appears larger and the blockade can be partly lifted due to electron hopping via edge states. As a consequence, we should observed a reduction of the CO period when the parallel conduction mechanism is increased. This effect is observed experimentally and provides a method for extracting the real size of the dot as well as the size of the localizing region.

In a region affected by trapping at the edge states but where Coulomb peaks are still clear and distinct, the largest Coulomb diamonds provide an estimate for the minimum effective dot size (all traps filled), whereas the smallest diamonds give the maximum dot size (all traps empty). From this, we obtain a diameter of 58 with 14 nm extent for the localizing region. The presence of traps at the edge of the structure, thus provides an effective mechanism for dot compression.

The quantum dot compression is more directly demonstrated by the change of the excited state energy with gate voltage, as the mean on particle level spacing Δ_1 is inversely proportional to the dot size (figure B.3(a)). Indeed, this observation discards the possibility that the change in the shape of the Coulomb diamonds could be due to an increase of conductivity due to a modification of the tunneling barrier profile and, so of the electron tunneling rates. By neglecting the non-uniformity in the doping concentration, Δ_1 can be estimated by equating the spatial extension of the ground state to the SET dot radius R for a 2D isotropic harmonic oscillator confinement [36]:

$$\tfrac{1}{2}m^{\star}{\omega_0}^2R^2 = \hbar\omega_0 = \Delta_1, \tag{B.1}$$

where $m^{\star} = 0.19m_{e-}$ the transverse mass of electron in silicon and $\hbar\omega_0$ the quantum dot confinement energy.

For example, in the range $3.3 < V_G < 3.7$ V, we obtain $E_C \sim 4.4$, 3.2 and 2.1 meV and $\Delta_1 \sim 2.1$, 1.7 and 1.1 meV from which we obtain a dot size of about 30, 39 and 58 nm, respectively, for $V_G = 3.35$, 3.45 and 3.55 V. This is in good agreement with the absence of a depletion at $V_G = 3.55$ V and a depletion width of 14 nm for $V_G = 3.35$ V.

Finally, it is interesting to notice that the extrapolation of the charging energy in the region where Coulomb diamonds disappear (conduction via edge states) lead to a value ∼1.0 meV similar to the excited states energy for a dot size of 58 nm.

[3] The dimensionless interaction parameter r_s usually characterizes the relative strength of Coulomb interaction in a structure. In a 2D quantum dot, it is related to the electron density n_s by $r_s = (\pi n_s)^{-1/2}/a_0$ where $a_0 = \hbar^2\epsilon/(me^2)$ is the effective Bohr radius and, m and ϵ are, respectively, the electron effective mass and the dielectric constant in silicon.

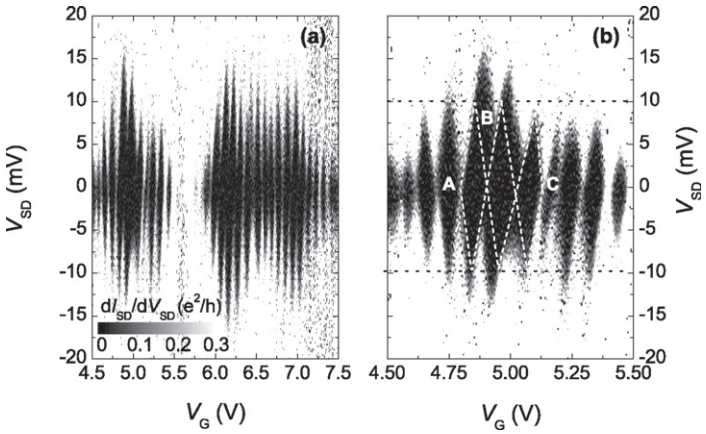

Figure C.1. (a) Differential conductance $\mathrm{d}I_{\mathrm{SD}}/\mathrm{d}V_{\mathrm{SD}}$ versus V_{G} and V_{SD} at $V_{\mathrm{C1}} = 0.5$ V. (b) Close-up view of Coulomb diamonds structure. In some cases, the first-order tunneling is strongly suppressed (B) compared with expected diamonds (A). (C) shows a charging by a single impurity in the SET island.

Appendix C. Tunneling and trap-assisted cotunneling

In regions of gate voltages where the IDQD lines are not present and the conductivity not affected by the trap occupancy (diamond A in figure C.1(b)), the SET charging energy can equivalently be calculated by measuring the width of a Coulomb diamond along V_{G} or along V_{SD} and converting the corresponding voltages into energies by using the value of the level arm, respectively, for the SET gate, e.g. $\alpha_{\mathrm{G}} = C_{\mathrm{G}}/C_{\Sigma}$ or the SET drain e.g. $\alpha_{\mathrm{D}} = C_{\mathrm{D}}/C_{\Sigma}$. We find $E_{\mathrm{C}} \sim 4.4$ meV using α_{G} and 4.2 meV using α_{D}.

For the diamond A, when the SET dot is blocked for conduction, the source–drain current follows $I_{\mathrm{SD}} \propto V_{\mathrm{SD}}^{\beta}$ with $\beta = 3$ as expected for single electron tunneling through a two-tunnel junction because of cotunneling effect [37]. On the other hand, when a large number of traps at the edge of the SET are occupied (diamond B in figure C.1(b)), we found $\beta = 9$ and diamond widths along V_{SD} that extend well over the expected charging energy. The periodicity along V_{G} is also locally lost at zero source–drain bias.

Although we observe a small variation in the values of capacitances and charging energy from peak to peak, a possible variation in the mean one-particle level spacing is not sufficient to explain the previous observation. However, a correct estimate of the charging energy and period could be obtained if one consider an anomalous suppression of cotunneling at the edge of the diamonds [38]. As previously discussed, when all traps are filled, cotunneling via traps at the periphery is suppressed because vacant states are not available and Coulomb repulsion too strong for electron to tunnel directly via the SET island.

From the expected value for the charging energy, one can estimate that inelastic cotunneling is associated with an energy difference of 1.5 meV, a value close to the mean single particle level spacing estimated in the same region (∼1.8 meV). Because electron motion in the IDQD is associated with tunneling via traps at the edge of the SET, this energy value has to be compared to the value of the charging energy at the shift region.

To this end, we have used of the second IDQD gate that was previously grounded. The SET current is first mapped as a function of V_{G} and V_{C1} with $V_{\mathrm{C2}} = 0$ to choose a low noise

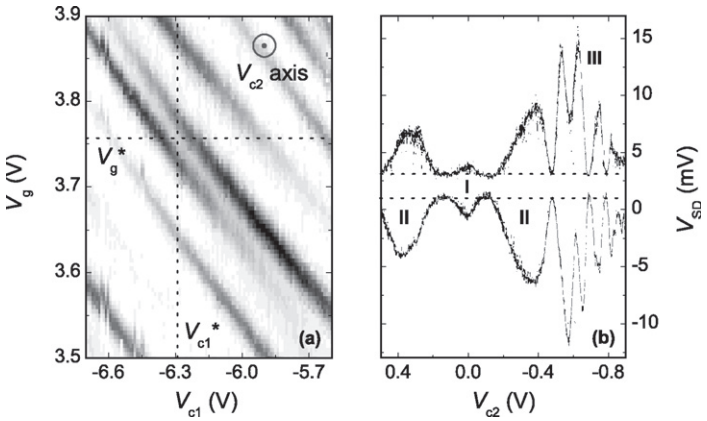

Figure C.2. (a) Example of a Coulomb peak shift for $V_{C2} = 0$. (b) Contour plot at $I_{SD} = I_{SD}\left(V_g^\star, V_{C1}^\star\right)$ showing coulomb diamonds as a function of V_{C2}.

region where a well defined shift is present and determine the IDQD–SET lines crossing point $V_{C1}^\star = -6.3\,\text{V}$ and $V_G^\star = 3.76\,\text{V}$ (figure C.2(a)). In this region, the mean energy level spacing is about 1.1 meV. In this experimental configuration, the variation of I_{SD} with V_G and V_{C2} for $V_{C1} = V_{C1}^\star$ has similar behavior as in figure C.2(a), and a clear shift centered on $V_{C2} = 0$ is obtained. Because of its position, away from the SET island, V_{C2} can be used to detune the IDQD states from the degeneracy point without significantly affecting the SET at low biases. Coulomb diamonds are then obtained by varying V_{C2} across 0 V with $V_G = V_G^\star$ and $V_{C1} = V_{C1}^\star$ (figure C.2(b)).

The pattern of Coulomb diamonds is formed by a central diamond (I) with a charging energy of 2.1 meV (between the two IDQD states), with two large-side diamonds (II). These are followed by usual Coulomb diamonds (III) that are associated with the direct influence of V_{C2} on the SET ($V_{C2} > 0.5\,\text{V}$). The asymmetric shape of the diamonds (II) may be attributed to a difference in the charge polarization and the charge tunneling rates [39]. At the IDQD–SET line crossing, the first-order tunneling is suppressed and the conductivity is limited by higher orders of tunneling as explained in the previous sections. In figure C.2(b), the onset for conductivity gives an indication on the energy scale involved in the inelastic cotunneling process. Its value is closed to 1.0 meV and, as expected, similar to the mean single particle energy spacing estimated for a 60 nm diameter quantum dot (1.1 meV).

These results, together with the observation of excited states in the device and the understanding of internal dynamics in the IDQD–SET-trap system, are consistent with the fact that the inelastic cotunneling via edge states is responsible for the observation of IDQD lines and, under appropriate coupling, the presence of shifts at specific value of gate voltages. The activation energy for the traps at the edge is varying between 1 and 2 meV typically.

References

[1] Lambe J and Jaklevic R C 1969 *Phys. Rev. Lett.* **22** 1371
[2] Averin D V and Likharev K K 1986 *J. Low Temp. Phys.* **62** 345
[3] Fulton T A and Dolan G J 1987 *Phys. Rev. Lett.* **59** 109
Lafarge P, Pothier H, Williams E R, Esteve D, Urbina C and Devoret M H 1991 *Z. Phys.* B **85** 327

[4] Martinis J M, Nahum M and Jensen H D 1994 *Phys. Rev. Lett.* **72** 904
[5] Guo L, Leobandung E and Chou S Y 1997 *Science* **275** 649
[6] Grossing G and Zeilinger A 1988 *Complex Syst.* **2** 197
Grossing G and Zeilinger A 1988 *Complex Syst.* **2** 611
[7] Warren W S 1997 *Science* **277** 1688
Shnirman A, Schön G and Hermon Z 1997 *Phys. Rev. Lett.* **79** 2371
Steane A 1997 *Appl. Phys.* B **64** 623
Takeuchi S 2000 *Phys. Rev.* A **62** 032301
Loss D and DiVincenzo D P 1998 *Phys. Rev.* A **57** 120
[8] Averin D V and Likharev K K 1991 *Mesoscopic Phenomena in Solids* vol 30 (New York: North-Holland) chapter 6 p 208
Averin D V and Nazarov Yu V 1990 *Phys. Rev. Lett.* **65** 2446
[9] Berman D, Zhitenev N B, Ashoori R C, Smith H I and Melloch M R 1997 *J. Vac. Sci. Technol.* B **15** 2844
[10] Meirav U, Kastner M A and Wind S J 1990 *Phys. Rev. Lett.* **65** 771
Kouwenhoven L P, van der Vaart N C, Johnson A T, Kool W, Harmans C J P M, Williamson J G, Staring A A M and Foxon C T 1991 *Z. Phys.* B **85** 367
Pothier H, Lafarge P, Orfila P F, Urbina C, Esteve D and Devoret M H 1991 *Physica* B **169** 573
[11] Huang X *et al* 1999 *IEDM Tech. Dig.* p 67
[12] Fujiwara A, Inokawa H, Yamazaki K, Namatsu H, Takahashi Y, Zimmerman N M and Martin S B 2006 *Appl. Phys. Lett.* **88** 053121
Angus S J, Ferguson A J, Dzurak A S and Clark R G 2007 *Nanoletters* **7** 2051
[13] Buehler T M, Reilly D J, Starrett R P, Kenyon S, Hamilton A R, Dzurak A S and Clark R G 2003 *Microelectron. Eng.* **67–68** 775
Buehler T M, Reilly D J, Brenner R, Hamilton A R, Dzurak A S and Clark R G 2003 *Appl. Phys. Lett.* **82** 577
[14] Matsuoka H and Kimura S 1995 *Appl. Phys. Lett.* **66** 613
Yano K, Ishii T, Hashimoto T, Kobayashi T, Murai F and Seki K 1994 *IEEE Trans. Electron Devices* **41** 1628
Takahashi Y, Nagase M, Namatsu H, Kurihara K, Iwadate K, Nakajima Y, Horiguchi S, Murase K and Tabe M 1995 *Electron. Lett.* **31** 136
[15] Hofmann F, Heinzel T, Wharam D A, Kotthaus J P, Böhm G, Klein W, Tränkle G and Weimann G 1995 *Phys. Rev.* B **51** 13872
Pierre M, Wacquez R, Roche B, Jehl X, Sanquer M, Vinet M, Prati E, Belli M and Fanciulli M 2009 *Appl. Phys. Lett.* **95** 242107
Yamahata G, Tsuchiya Y, Mizuta H, Uchida K and Oda S 2009 *Solid State Electron.* **53** 779
[16] Hasko D G *et al* 2008 *Appl. Phys. Lett.* **93** 192116
[17] Zhitenev N B, Brodsky M, Ashoori R C, Pfeiffer L N and West K W 1999 *Science* **285** 715
[18] Gunther A, Khoury M, Miličcić S, Vasileska D, Thornton T and Goodnick S M 2000 *Superlattices Microstruct.* **27** 373
[19] Morello A, Escott C C, Huebl H, Willems van Beveren L H, Hollenberg L C L, Jamieson D N, Dzurak A S and Clark R G 2009 *Phys. Rev.* B **80** 081307
Morello A, Escott C C, Huebl H, Willems van Beveren L H, Hollenberg L C L, Jamieson D N, Dzurak A S and Clark R G 2010 *Nature* **467** 687
[20] Wasshuber C, Kosina H and Selberherr S 1997 *IEEE Trans. Comput.-Aided Des. Integr. Circuits Syst.* **16** 937
[21] Nabor K, Kim S and White J 1992 *IEEE Trans. Microw. Theory Tech.* **40** 1496
[22] Lee K H, Greentree A D, Dinale J P, Escott C C, Dzurak A S and Clark R G 2005 *Nanotechnology* **16** 74
[23] Kawata Y, Khalafalla M A H, Usami K, Tsuchiya Y, Mizuta H and Oda S 2007 *Japan. J. Appl. Phys.* **46** 4386
[24] Fujisawa T, Hayashi T, Hirayama Y, Cheong H D and Jeong Y H 2004 *Appl. Phys. Lett.* **84** 2343
[25] Rossi A, Ferrus T, Podd G J and Williams D A 2010 *Appl. Phys. Lett.* **97** 223506
[26] Hofmann F, Heinzel T, Wharam D A, Kotthaus J P, Bohm G, Klein W, Trankle G and Weimann G 1995 *Phys. Rev.* B **51** 13872

[27] Müller H-O, Furlan M, Heinzel T and Ensslin K 2001 *Europhys. Lett.* **55** 253
[28] Pepper M 1977 *Proc. R. Soc.* A **353** 225
[29] Rudin A M, Guo L J, Glazman L I and Chou S Y 1998 *Appl. Phys. Lett.* **73** 3429
[30] Altermatt P P, Schenk A and Heiser G 2006 *J. Appl. Phys.* **100** 113714
[31] Abrahams E, Anderson P W, Licciardello D C and Ramakrishnan T V 1979 *Phys. Rev. Lett.* **42** 673
[32] Thomson J J 1910 *Phil. Mag.* **20** 752A
Benninghoven 1969 *Phys. Status Solidi* **34** K169
[33] Lau F, Mader L, Mazure C, Werner C and Orlowski M 1989 *Appl. Phys.* A **49** 671
[34] Guo L J and Chou S Y 1998 *Electron. Lett.* **34** 1031
[35] Kodera T, Ferrus T, Nakaoka T, Podd G, Tanner M, Williams D and Arakawa Y 2009 *Japan. J. Appl. Phys.* **48** 06FF15
[36] Tilke A T, Simmel F C, Blick R H, Lorenz H and Kotthaus J P 2001 *Prog. Quantum Electron.* **25** 97
[37] Averin D V and Odintsov A A 1989 *Phys. Lett.* A **140** 251
Geerligs L J, Averin D V and Mooij J E 1990 *Phys. Rev. Lett.* **65** 3037
[38] Luo X, Tomcsanyi M, Orlov A O, Kosel T H and Snider G L 2006 *Appl. Phys. Lett.* **89** 043511
[39] Tager A A, Xu J M and Moskovits M 1997 *Phys. Rev.* B **55** 4530